LAWRENCE
LIVERMORE
NATIONAL
LABORATORY

LLNL-CONF-615532

A geomechanical mechanism that counteracts flow channeling induced by reservoir thermal drawdown

P. Fu, Y. Hao, C. R. Carrigan

February 4, 2013

Stanford Geothermal Workshop 2013
Sanford, CA, United States
February 11, 2013 through February 13, 2013

Disclaimer

PROCEEDINGS, Thirty-Eighth Workshop on Geothermal Reservoir Engineering
Stanford University, Stanford, California, February 11-13, 2013
SGP-TR-198

A GEOMECHANICAL MECHANISM THAT COUNTERACTS FLOW CHANNELING INDUCED BY RESERVOIR THERMAL DRAWDOWN

Pengcheng Fu, Yue Hao, and Charles R. Carrigan

Atmospheric, Earth, and Energy Division, Lawrence Livermore National Laboratory
7000 East Ave., L-286
Livermore, CA 94550, USA
e-mail: fu4@llnl.gov

ABSTRACT

This study employs a coupled thermal–hydrologic–mechanical (THM) model to investigate flow channeling associated with reservoir thermal drawdown. Flow channeling refers to the phenomenon that the fractures carrying more flow tend to cool faster and may subsequently dilate more than fractures carrying less flow, thereby causing increasingly severe flow concentration into the a small number of fractures. Our study discovers that the anisotropic thermal stress in a cooling reservoir tends to loosen fractures that are normal to the primary flow direction more than do fractures along the primary flow direction. This mechanism can counteract the flow channeling potential by promoting a diffuser flow pattern. We also found that the significance of the effects of this mechanism dependent on certain inherent characteristics of the fracture network. Fracture network patterns that are prone to and those with strong inherent resistance to flow channeling need to be identified.

INTRODUCTION

During the production phase of an engineered geothermal system (EGS) in fractured rock, reservoir temperature gradually decreases, which is termed "thermal drawdown" [Bödvarsson and Tang, 1982]. The temperature change in the rock induces a thermal stress increment (termed thermal stress in the rest of the paper) on top of the original *in situ* stress. Whereas the thermal stress increment in cooled rock is generally tensile, it could be compressive in the rock body surrounding the cooled zone due to the effect of strain compatibility [Ghassemi et al., 2007; Koh et al., 2011]. This causes the overall compressive stress in the cooled rock body to decrease and the conducing fractures becomes less tights (i.e. greater permeability). It has been observed in the field that the system hydraulic impedance between the injection and production wells decreases with heat production [Kohl et al., 1995; Bruel 2002]. Because the rock surrounding fractures that conduct a larger proportion of fluid flow cools faster than that surrounding fractures with lower flow rate, a practical concern is that this mechanism will further increase the permeability of the fractures that are already conducting the majority of the flow compared with other fractures in the network. This may cause flow channeling, namely flow concentrating into a small number of fractures [Hicks et al., 1996; Koh et al., 2011]. This effect is potentially detrimental to the performance of a geothermal system, because only the heat in rock around a few highly permeable fractures can be extracted, resulting in a small volume of accessible hot rock in the reservoir.

In this paper, we first present a numerical model for coupled thermal–hydrologic–mechanical (THM) simulation. The flow channeling phenomenon is quantitatively investigated using the numerical model. The main objectives include to identify physical mechanisms involved in flow channeling and to study fracture network characteristics that affect flow channeling potentials.

COUPLED THM MODEL

Simulation Strategy and Framework

Different phenomena at different stages of the life cycle of an EGS reservoir are controlled by different physical processes and associated with different time scales. For instance, hydraulic fracturing concerns time scales from minutes to hours, hydraulic shearing concerns hours to days, and the physical processes dealt with in the current study spans from months to years [Bruel 2002; Taron et al., 2009]. Therefore, the simulation strategy needs to be tailored and optimized for each stage to capture relevant physical mechanisms. The model used in this study is related to the hydraulic fracturing and hydraulic shearing models [Fu et al., 2012a and 2012b] that we have developed, but modifications and improvements as described in the present paper are necessary for simulating long-term THM phenomena. In both hydraulic fracturing and hydraulic shearing, temperature change in the reservoir can be ignored

but the transient evolution of fluid pressure in the fracture network must be modeled. Reservoir temperature change becomes an important consideration when relatively long term production is modeled. As the temperature evolution takes place at a rather slow rate, we can adopt a relatively large time step and assume the fluid flow in the fracture network to be at a steady state during each time step, which is an assumption commonly adopted [Hicks et al. 1996].

The numerical model consists of several modules as shown in Figure 1. In each time step, they are sequentially invoked as follows. First the discrete fracture network (DFN) –based fluid flow solver is used to solve for the flow field under the given boundary condition. Because a critical characteristic in DFN flow is the dependence of fracture aperture (which determines permeability) on fluid pressure, the flow solver and a rock joint model, which quantifies this dependency, are invoked iteratively until the solution converges. The fracture aperture distribution from the DFN model is then mapped onto a finite difference mesh to obtain the equivalent permeability field to be used by the continuum-based thermal-hydrological model (the TH model). The TH model simulates both fluid flow and heat flow, and updates the temperature field to the beginning of the next time step. This temperature field is used by a solid finite element model (FEM) to obtain the thermal stress increment tensor, which is then mapped onto the DFN network to update the total stress on each fracture segment. The next time step then begins with the updated stress field.

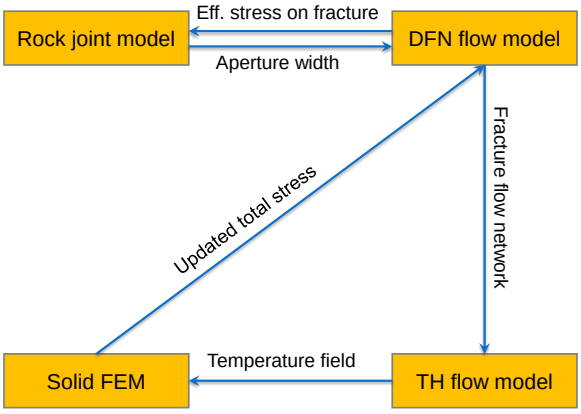

Figure 1: Main modules in the coupled THM model.

DFN Flow Solver

The DFN flow solver discretizes a given fracture network into flow cells, which are line segments in 2D. The solvers use an implicit finite element formulation which is fairly routine and not described here. The aperture width w is calculated based on the Barton-Bandis model [Bandis et al., 1983; Barton et al., 1985] as a function of the effective normal stress σ'.

$$\sigma' = \frac{w_{max} - w}{A - B(w_{max} - w)} \quad (1)$$

where w_{max} is the aperture width at the zero-effective stress state, which is essentially the *maximum joint closure* in the original joint model of Bandis et al. [1983]; A and B are two material constants. If we identify a second reference state with effective normal stress σ'_{ref} and aperture width w_{ref}, the two material can be calculated as

$$A = w_{max} \frac{w_{max} - w_{ref}}{\sigma_{ref} w_{ref}} \text{ and } B = \frac{w_{max} - w_{ref}}{\sigma_{ref} w_{ref}} \quad (2)$$

The effective stress (compression is positive) is the difference between the total normal stress σ_n acting on the fracture segment by the rock matrix and the fluid pressure P inside the fracture as $\sigma' = \sigma_n - P$.

Continuum-Based TH Model

The Non-isothermal Unsaturated Flow and Transport (NUFT) code developed at the Lawrence Livermore National Laboratory (LLNL) serves as the thermal-hydrological module. NUFT has been developed to capture multiphase, multi-component heat and mass flow, and reactive transport in unsaturated and saturated porous media [Nitao 1998]. An integrated finite-difference spatial discretization scheme is used to solve mass and energy balance equations in both flow and reactive transport models. The resulting nonlinear equations are solved by the Newton-Raphson method. The adaptation of NUFT, a continuum-based model, for the simulation of DFN flow as well verification and validation cases is described in a companion paper [Hao et al., 2013] and not repeated here.

Thermal Stress Calculation

The rock mass is assumed to be linearly elastic, and the principle of superposition applies. Therefore the thermal stress can be calculated in a separate model and superposed onto the original *in situ* stress. The thermal stress calculation is performed in the finite element solid solver in GEOS [Settgast et al., 2012], another LLNL code, and the procedure described in section 2.10 of Cook et al. [2001] is followed. The finite element mesh used for thermal stress calculation has to be large enough to properly take the effects of the large rock medium (that can be considered infinite) into consideration. Note that the DFN mesh, the finite difference NUFT mesh, and finite element GEOS mesh need not to be conforming, as long as variable mapping between them is appropriately handled. Once the total stress tensor (the summation of the original *in situ* stress and the thermal stress) is obtained, to calculate the total normal stress on each fracture segment (i.e. a

flow cell in the DNF mesh) only involves trivial tensor operations.

ANISOTROPY IN THERMAL STRESS

The core mechanism discussed in the paper is closely related to the anisotropic thermal stress rising in geothermal reservoirs. Before presenting the numerical simulation results, we first consult a closed-form solution in a highly idealized setting to gain some insight into the nature of this mechanism.

Assume in a 2D (plane-strain) originally homogeneous infinite space, an elliptical zone at the center experiences a temperature decrease of ΔT whereas the temperature in the remainder of the medium remains unchanged. The lengths of the two major axes of the elliptical zone are 2a and 2b, along the *x*- and *y*- axes, respectively, as shown in Figure 2. It has been proved (Mindlin and Cooper, 1950) that inside this cooling zone the thermal stress rising from the temperature difference is homogeneous. The two components are

$$\sigma_x^T = -\frac{bE\Delta T\alpha_L}{(a+b)(1-\nu)} \quad (3)$$

$$\sigma_y^T = -\frac{aE\Delta T\alpha_L}{(a+b)(1-\nu)} \quad (4)$$

where E is the Young's modulus of the medium, ν is the Poisson's ratio, and α_L is the coefficient of thermal expansion (linear). Both components are negative because it is customary to define compression stress as positive in geomechanics. These results shows that even in isotropic materials, thermal stress can be highly anisotropic as a result of the shape of the cooling zone. How this phenomenon affects the evolution of flow patterns in fractured EGS reservoir will be discussed below along with numerical examples.

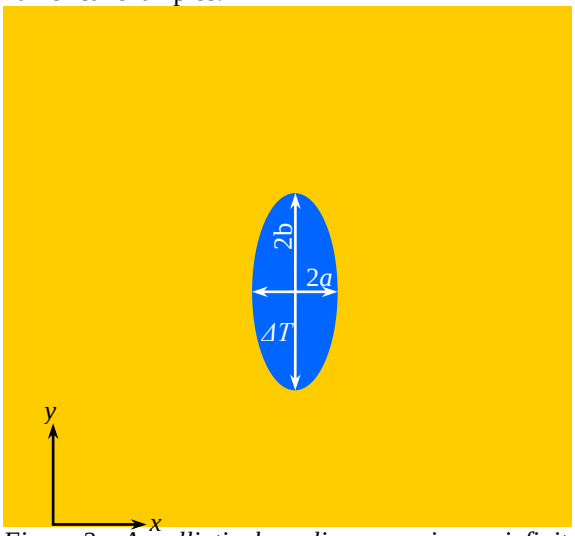

Figure 2: An elliptical cooling zone in an infinite medium.

BASELINE NUMERICAL EXAMPLE

Initial condition of the reservoir

In this 2D model, the two orthogonal fracture sets in the EGS reservoir form a regular grid as shown in Figure 3. The 2D coordinate system is established so that the *x*-axis points east and the y-axis points north. We term the fracture set parallel to the *x*-axis the *x*-set and the other the *y*-set. The domain as well as the fracture network is assumed to be infinite, and the numerical model is made large enough to reasonably represent behavior of an infinite domain. Fracture spacing for both sets is 20 meters. The production well is 400 m north of the injection well, and each well is at an intersection of two orthogonal fractures. The injection rate and production rate both remain constant at 0.06 L/s/m, which is equivalent to 2.25 bpm per 100 m thick reservoir. Some other parameters for the model are presented in Table 1.

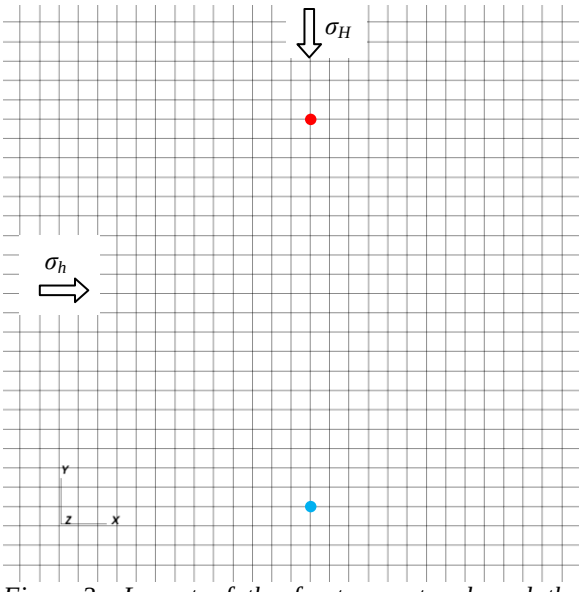

Figure 3: Layout of the fracture network and the injection (blue dot) and production (red dot) wells. Note that only the center portion of the computational domain is shown.

Reservoir Behavior without Thermomechanical Effects

Although we use the same rock joint parameters for both sets, their initial apertures (i.e. permeability) are affected by the anisotropic *in situ* stress and thus not the same. According to the joint model described by equation (1), the original aperture widths for the *x*-set and y-set are 0.041 mm and 0.058 mm, respectively. The y-set has significantly higher permeability than the x-set, which is the primary motivation for the north-south well layout.

Table 1: Parameters for the baseline numerical model.

Parameter	Value
Original *in situ* stress	$\sigma_h = \sigma_x^0 = 17$ MPa (e-w) $\sigma_H = \sigma_y^0 = 25$ MPa (n-s)
Original pore pressure	P_0 = 15 MPa.
Rock joint parameters	w_{max} = 0.5 mm σ_{ref} = 20 MPa w_{ref} = 0.05 mm
Initial reservoir temperature	T_0 = 150°C
Injection fluid temperature	T_i = 50ºC
Mechanical properties of rock	E = 20 GPa ν = 0.2
Thermal properties of rock	Conductivity K_r = 3 W/m/°C Heat capacity C_r = 2.5 MJ/m^3/°C
Fluid properties	Those of water.

According to the results of the DFN flow model, the initial flow pattern before significant thermal drawdown has taken place (i.e. no thermal stress) is visualized in Figure 4. In this fracture configuration, a *y*-set fracture, except the one directly connects the two well, must be fed by *x*-set fractures. Because the *x*-set fractures act like bottlenecks in the fracture network due to the high total stress acting on them, flow tends to concentrate in a few *y*-set fractures. At the east-west cross section halfway between the two wells, the five *y*-set fractures at the center of the model carry more than 50% of the overall flow between the two wells.

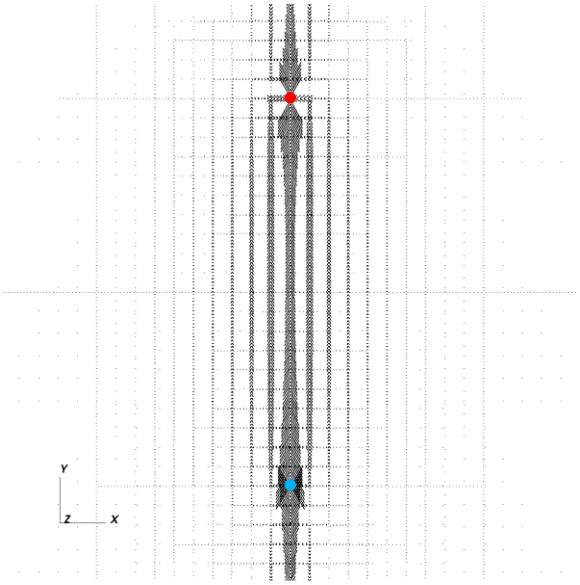

Figure 4: Flow from the injection well to the production well. The orientation of the arrows indicates flow direction, and the size of the arrows is proportional to the flow rate.

If we ignore the effects of the thermomechanical effects rising along with the production and keep the fracture aperture width distribution unchanged from this initial condition, we can use NUFT to directly predict the temperature field evolution in the reservoir without going through the loop shown in Figure 1. The predicted temperature distribution 10 and 20 years after production has commenced is shown in Figure 5.

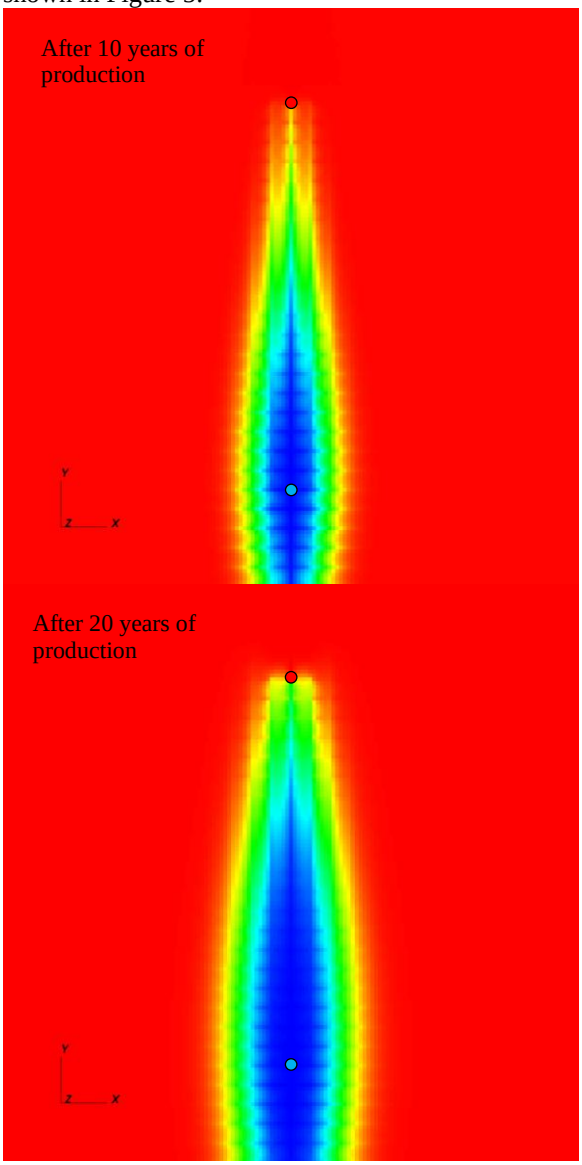

Figure 5: Temperature distribution in the reservoir after 10 and 20 years of production, if the thermomechanical effects are ignored. 150°C and 50ºC are at the two ends of the color map.

Reservoir Behavior with Thermomechanical Effects

As shown in Figure 5, the cooling zone in this case tends to elongate along the primary flow direction, namely the y-direction. The coupled THM simulation predicts a temperature distribution after 10 years of production as shown in Figure 6, which is somewhat different from that in Figure 5 but the elongation direction of the cooling zone unchanged. At this state, the absolute value of the thermal stress induced is shown in Figure 7. The magnitude of the thermal stress in the *y*-direction is much greater than that in the *x*-direction, which is consistent with the thermal stress solution for an elliptical cooling zone.

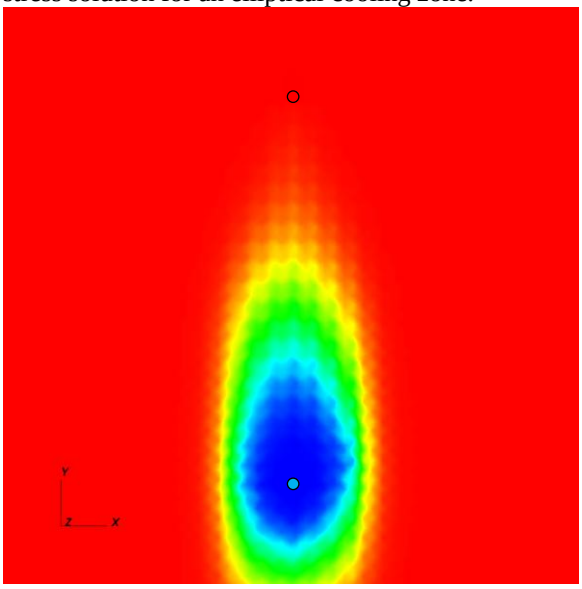

Figure 6: Temperature distribution in the reservoir after 10 years of production, with the effects of thermal stress taken into account.

Because the thermal stress increment loosens the *x*-set fractures more than it loosens the *y*-set fractures, the overall flow pattern continuously evolves from the initial pattern shown in Figure 4, and the updated flow pattern after 10 years is shown in Figure 8. As the permeability of the *x*-set fractures near the injection well increases, thanks to the high thermal stress in the *y*-direction, the system is able to feed flow into y-set fractures farther from the well. Consequently, the flow pattern becomes diffuser and the cooling zone becomes wider than the scenario ignoring the thermomechanical effects.

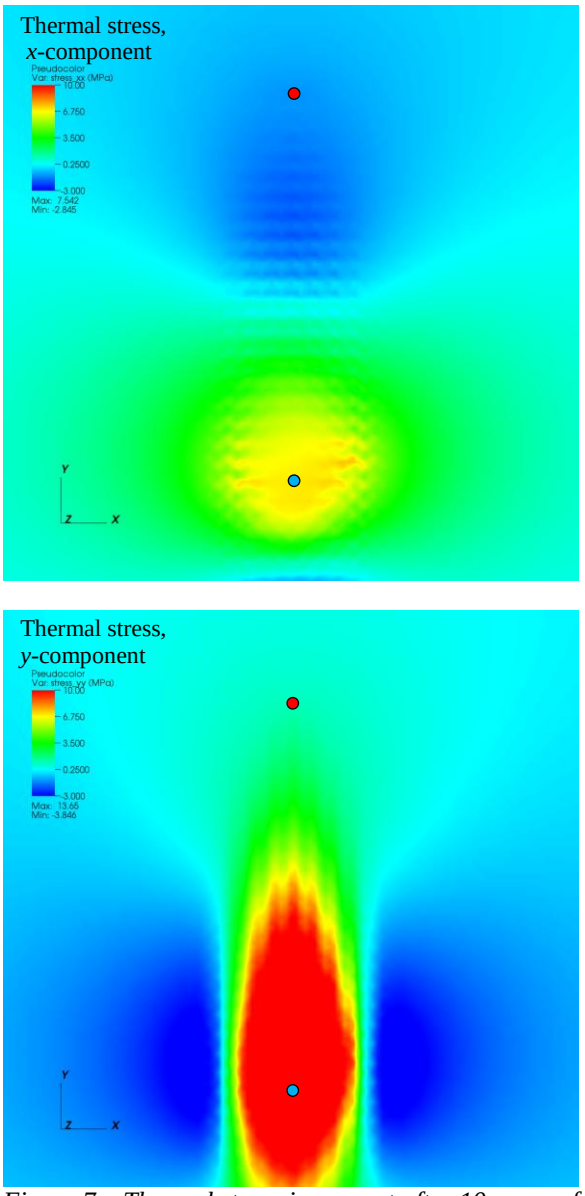

Figure 7: Thermal stress increment after 10 years of production. Note that in this figure traction is positive.

The evolution of the production temperature is shown in Figure 9. Both the scenario ignoring thermomechanical effects and that taking the thermal effects into account are shown. The production temperature history is substantially affected by the effects of the thermal stress. The thermomechanical effects remarkably delay the time of thermal breakthrough. However, once the breakthrough takes place, the temperature decline is much faster than that with the thermomechanical effects ignored.

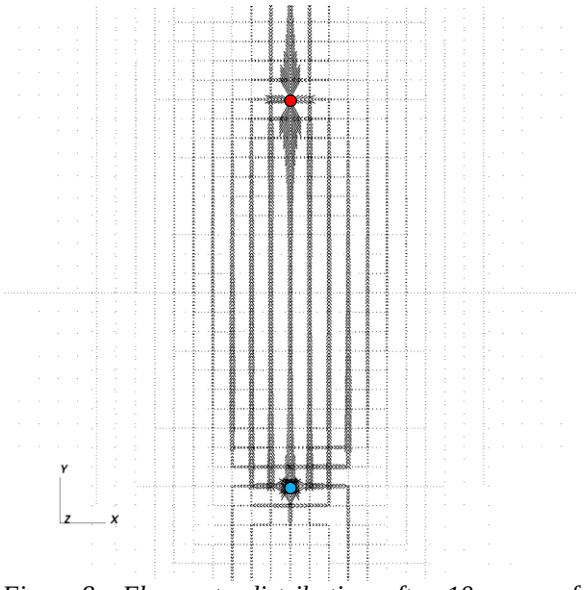

Figure 8: Flow rate distribution after 10 years of production, with the effects of thermal stress considered.

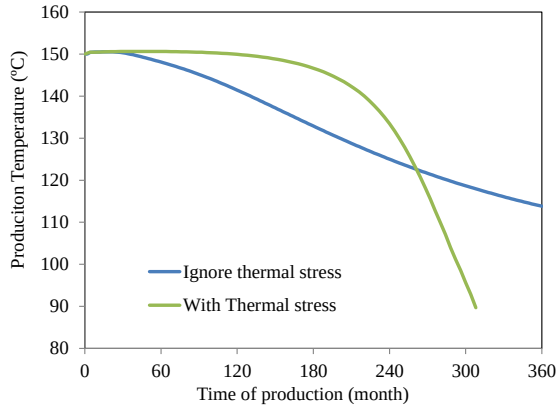

Figure 9: Production temperature evolution for the regular grid scenario.

NUMERICAL EXAMPLES FOR RANDOM FRACTURE NETWORK

Random Fracture Network Features

We have used a highly idealized fracture network pattern to illustrate the significance of effects of thermal stress. In this section, we perform similar simulation and analysis on randomly generated fracture network patterns. The two patterns generated are shown in Figure 10. In pattern A, the fracture orientation follows a uniform distribution along all possible orientations. Pattern B consists of two fracture sets. Fractures in the first set (x-set) are oriented between 0 and 5° rotating counterclockwise from the x-axis, and the second set (y-set) between 80° and 85°. For both patterns, individual fractures are between 50 m and 150 m long. The total fracture length per unit area and the wellbore locations are the same as those for the baseline regular grid case. Because the fracture connectivity is weaker in these random networks than in the regular grid, the hydraulic impedance between the two well is higher. Using the DFN flow model, we find that the maximum achievable closed-loop flow rate is approximately 1/3 of that for the baseline case. Therefore, we applied a constant flow rate of 0.02 liter per second per meter thickness of the reservoir. To make the production time scale comparable to the baseline case, we artificially reduce the heat capacity of the rock to 1/3 of the value in Table 1.

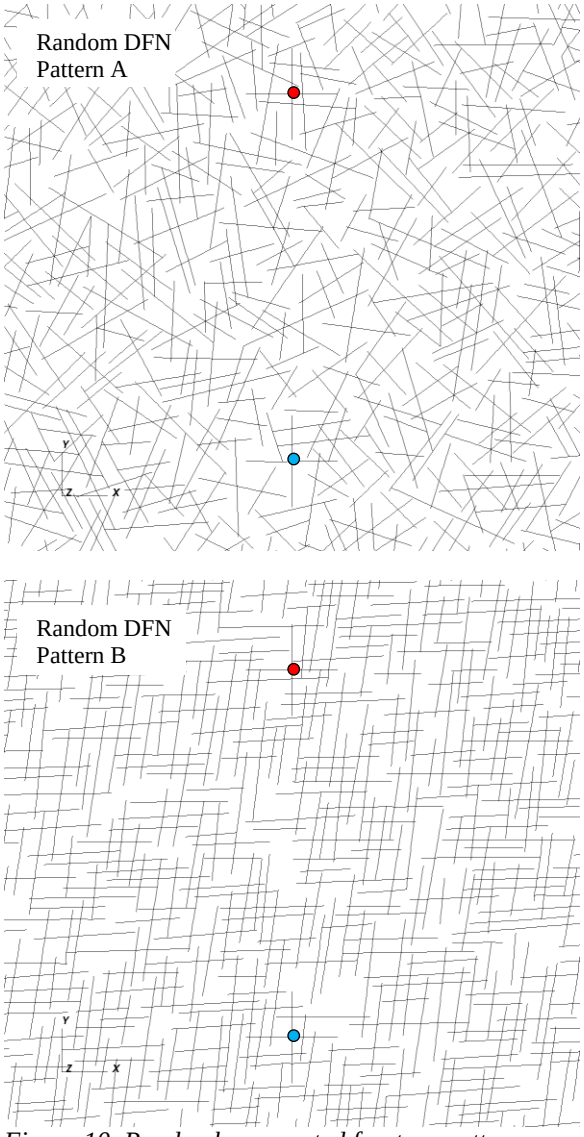

Figure 10: Randomly generated fracture patterns.

Simulation Results for Random DFN

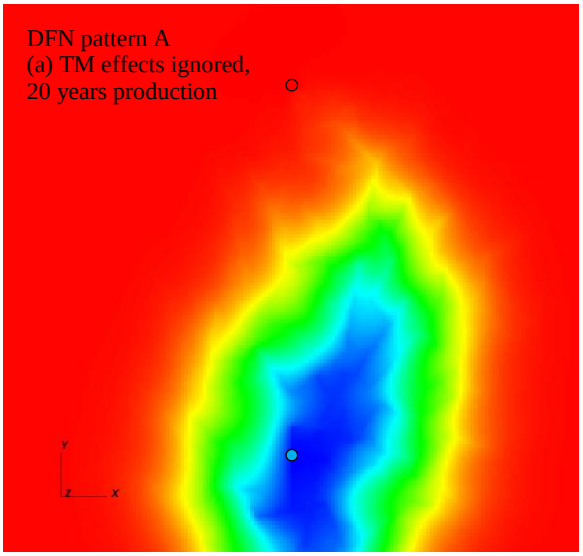

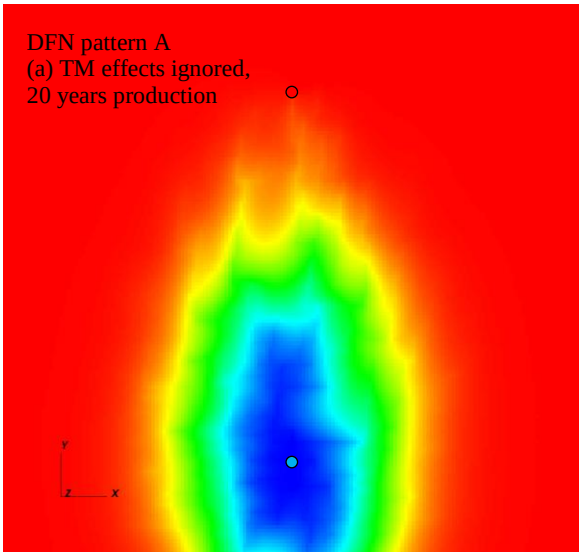

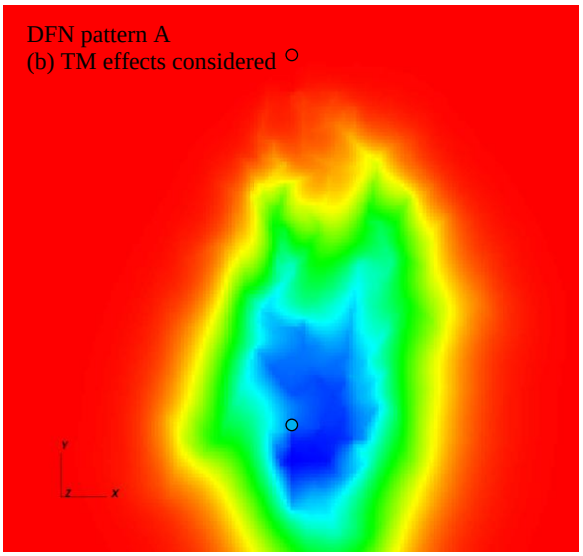

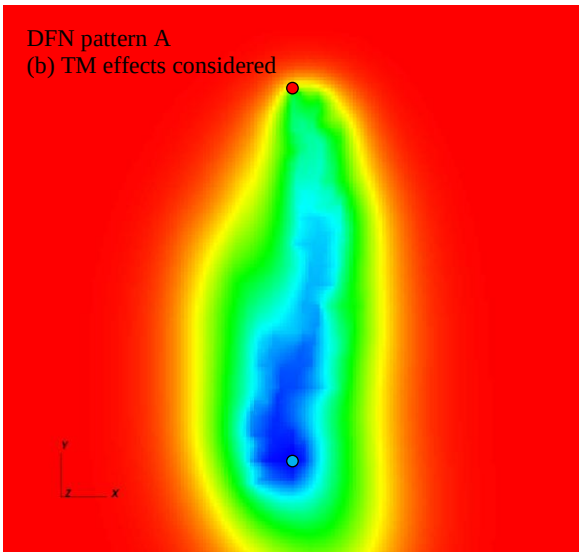

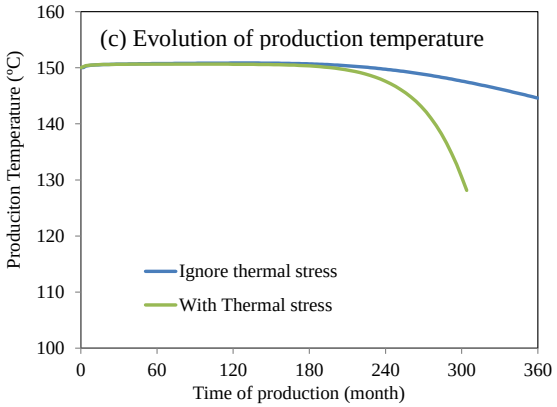

Figure 11: Simulation results for DFN pattern A.

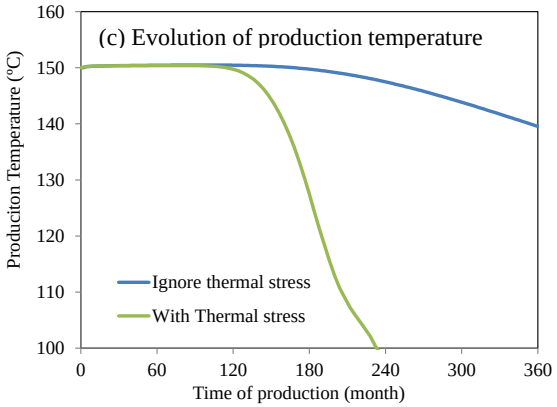

Figure 12: Simulation results for DFN pattern A.

The behaviors of the two random fracture networks are not only different from that of the regular grid network, but also significantly different from each other, despite their similarities in model parameters. For DNF pattern A, the two scenarios, namely with and without consideration of thermomechanical effects, reach thermal breakthrough approximately the same time, after 15 years of production. Prior to this, the themomechanical effects do not affect production temperature. Once thermal breakthrough takes place, the thermomechanical effects cause much quicker decline of temperature than that ignoring the thermomechanical effects, which is similar to what has been observed in the baseline regular grid case.

Simulation results for pattern B are similar to those of pattern A in that the thermomechanical effects do not seem to affect the breakthrough time but remarkably accelerate the post-breakthrough temperature decline. However, the flow channeling phenomenon is more evident for DFN pattern B than for pattern A, as the cooling zone becomes narrower in the *x*-direction after the thermomechanical effects are taken into account.

CONCLUSIONS

In this study, we used a coupled THM model to study the long term thermomechanical effects due to thermal drawdown on EGS reservoir performance. We compared fully coupled simulation results with those with thermal-mechanical coupling turned off to quantify the thermomechanical effects, particularly on the potential of flow channeling. An important discovery is a geomechanical mechanism that counteracts the flow channeling potential due to thermal drawdown. This mechanism arises from the fact that the anisotropic thermal stress tends to loosen the fractures normal to the primary flow direction, thereby promoting a diffuser flow pattern. The effects of this mechanism were found to be very significant for an idealized regular DFN pattern. However, to what extent this mechanism can reduce or delay flow channeling is dependent on basic characteristics of the fracture network. For two randomly generated networks investigated in this study, this mechanism was not able to significantly delay the time of thermal breakthrough. The flow channeling potential as well as engineering measures to prevent or delay flow channeling is being investigated.by the authors.

AUSPICES AND ACKNOWLEDGEMENTS

The authors gratefully acknowledge the Geothermal Technologies Program of the US Department of Energy for support of this work under the Enhanced Geothermal Systems Program. The authors also would like to acknowledge their collaborators at the Lawrence Livermore National Laboratory. Additional support provided by the LLNL LDRD project "Creating Optimal Fracture Networks" (#11-SI-006) is gratefully acknowledged. This work was performed under the auspices of the U.S. Department of Energy by Lawrence Livermore National Laboratory under Contract DE-AC52-07NA27344. This document has been released to unlimited external audience with an LLNL IM release number LLNL-CONF-615532.

REFERENCES

Barton, N., Bandis, S., and Bakhtar, K. (1985), "Strength, deformation and conductivity coupling of rock joints," *International Journal of Rock Mechanics and Mining Sciences & Geomechanics Abstracts*, 22(3), 121-140.

Bandis, S., Lumsden, A., and Barton, N. (1983), "Fundamentals of rock joint deformation," *International Journal of Rock Mechanics and Mining Sciences & Geomechanics Abstracts*, 20(6), 249-268.

Bödvarsson, G.S., and Tsang, C.F. (1982), "Injection and thermal breakthrough in fractured geothermal reservoirs," *Journal of Geophysical Research*, 87(B2), 1031–1048..

Bruel, D. (2002), "Impact of induced thermal stresses during circulation tests in an engineered fractured geothermal reservoir," Oil & Gas Science and Technology, 57(5), 459–470.

Cook, R.D., Malkus, D.S., Plasha, M.E., and Witt, R.J. (2001), *Concepts and Applications of Finite Element Analysis*, Fourth Edition, John Wiley & Sons.

Fu, P., Johnson, S.M., Hao, Y., and Carrigan, C.R. (2011), "Fully coupled geomechanics and discrete flow network modeling of hydraulic fracturing for geothermal applications." The 36th Stanford Geothermal Workshop, Jan. 31 – Feb. 2, 2011, Stanford, CA.

Fu, P., Johnson, S.M., and Carrigan, C.R. (2012), "An explicitly coupled hydro-geomechanical model for simulating hydraulic fracturing in arbitrary discrete fracture networks," *International Journal for Numerical and Analytical Methods in Geomechanics*, DOI: 10.1002/nag.2135.

Fu, P., and Carrigan, C.R. (2012), "Modeling responses of naturally fractured geothermal reservoir to low-pressure stimulation." The 36th Annual Meeting of Geothermal Resources Council, Sep. 30 - Oct. 3, 2012, Reno, NV.

Ghassemi, A., Tarasovs, S., and Cheng, A.H.-D. (2007), "A 3-D study of the effects of

thermomechanical loads on fracture slip in enhanced geothermal reservoirs," *International Journal of Rock Mechanics and Mining Sciences*, 44(8), 1132–1148.

Hao, Y., Fu, P., and Carrigan C.R. (2013), "Application of a dual-continuum model for simulation of fluid flow and heat transfer in fractured geothermal reservoirs," The 38th Stanford Geothermal Workshop, Feb. 11-13, 2013, Stanford, CA.

Hicks, T.W., Pine, R.J., Willis-Richards, J., Xu, S., Jupe, A.J., and Rodrigues, N.E.V.(1996), "A hydro-thermo-mechanical numerical model for HDR geothermal reservoir evaluation," *International Journal of Rock Mechanics and Mining Sciences & Geomechanics Abstracts*, 33(5), 499–511.

Koh, J., Roshan, H., and Rahman, S.S. (2011), "A numerical study on the long term thermo-poroelastic effects of cold water injection into naturally fractured geothermal reservoirs," *Computers and Geotechnics*, 38(5), 669–682.

Kohl, T., Evansi, K.F., Hopkirk, R.J., and Rybach, L. (1995), "Coupled hydraulic, thermal and mechanical considerations for the simulation of hot dry rock reservoirs," *Geothermics*, 24(3), 345–359.

Mindlin, R., and Cooper, H. (1950), "Thermoelastic stress around a cylindrical inclusion of elliptic cross-section", *ASME Journal of Applied Mechanics*, 17(3), 265–268.

Nitao, J.J. (1998), *Reference Manual for the NUFT Flow and Transport Code, Version 2.0.* Lawrence Livermore National Laboratory: Livermore, CA.

Settgast, R.R., Johnson, S.M., Walsh S.D.C., Fu, P., and Ryerson, F.J. (2012), "Simulation of hydraulic fracture networks in three-dimensions." *The 37th Stanford Geothermal Workshop*, Jan. 30-Feb. 1, 2012, Stanford, CA.